

Article

Airborne Brake Wear Debris: Size Distributions, Composition, and a Comparison of Dynamometer and Vehicle Tests

Paul G. Sanders, Ning Xu, Tom M. Dalka, and M. Matti Maricq

Environ. Sci. Technol., **2003**, 37 (18), 4060-4069 • DOI: 10.1021/es034145s

Downloaded from <http://pubs.acs.org> on November 18, 2008

More About This Article

Additional resources and features associated with this article are available within the HTML version:

- Supporting Information
- Links to the 4 articles that cite this article, as of the time of this article download
- Access to high resolution figures
- Links to articles and content related to this article
- Copyright permission to reproduce figures and/or text from this article

[View the Full Text HTML](#)



ACS Publications
High quality. High impact.

Airborne Brake Wear Debris: Size Distributions, Composition, and a Comparison of Dynamometer and Vehicle Tests

PAUL G. SANDERS, NING XU,
TOM M. DALKA, AND M. MATTI MARICQ*
Research Laboratory, Ford Motor Co., P.O. Box 2053,
MD 3083, Dearborn, Michigan 48121

Particle size distributions of light-duty vehicle brake wear debris are reported with careful attention paid to avoid sampling biases. Electrical low-pressure impactor and micro-orifice uniform deposit impactor measurements yield consistent size distributions, and the net particulate matter mass from each method is in good agreement with gravimetric filter measurements. The mass mean diameter of wear debris from braking events representative of urban driving is $6\ \mu\text{m}$, and the number-weighted mean is $1\text{--}2\ \mu\text{m}$ for three currently used classes of lining materials: low metallic, semimetallic, and non-asbestos organic (NAO). In contrast, the wear rates are very material dependent, both in number and mass of particles, with 3–4 times higher emissions observed from the low metallic linings as compared to the semimetallic and NAO linings. Wind tunnel and test track measurements demonstrate the appearance of micron size particles that correlate with braking events, with approximately 50% of the wear debris being airborne for the test vehicle in this study. Elemental analysis of the wear debris reveals a consistent presence of the elements Fe, Cu, and Ba in both dynamometer and test track samples.

Introduction

Current light-duty motor vehicle brake systems rely on friction to reduce vehicle speed. The majority of these systems utilize cast iron rotors and composite linings. The latter are available in a wide range of compositions aimed at meeting a variety of objectives including stopping distance, pedal feel, wear rate, and many others. The generation of particulate wear debris has received little attention, except indirectly in terms of the rotor and lining wear rates. Yet the wear debris is of interest for two reasons: It falls into the PM_{10} and $\text{PM}_{2.5}$ classes of ambient particulate matter (PM) that are regulated by the environmental agencies, and it deposits onto the wheel covers causing undesirable discoloration. The particles are chemically complex, including materials that range from organic binders to metals such as iron and copper.

The U.S. Environmental Protection Agency (EPA) includes brake wear particles in its MOBILE6 Particulate Emission Factor Model (1), and California does so in the similar EMFAC7g model. Both utilize a 13 mg/mi emission factor for PM_{10} brake wear debris, independent of brake lining composition, that can be traced back to the measurements

of Cha et al. (2) on asbestos brakes. However, the use of asbestos in brake linings has decreased considerably in the intervening two decades, and there is currently very limited information on the characteristics of the wear debris generated from modern linings (3, 4). The asbestos brakes have been replaced by a variety of new lining compositions that fall into three broad categories: non-asbestos organic (NAO), semimetallic, and low metallic. NAO linings are descendents of asbestos formulations but substitute potassium titanate fibers. They produce relatively low brake noise and have low wear rates but exhibit poor fade (the loss of braking efficiency during sustained high brake temperatures). Semimetallic linings, which have high steel fiber and iron powder content, perform with low wear and average fade but are generally noisier. Low metallic linings have a relatively high content of abrasives, resulting in high friction and good fade, but with the drawbacks of high wear rates and noise. The currently used 13 mg/mi emission factor qualitatively describes these brake emissions during urban driving; however, the present study shows that there is a factor of 4 variation in the emission rates between the different brake pad formulations.

The emphasis of our previous study (4) on brake wear was to describe the design of a dilution tunnel and isokinetic sampling system aimed at making accurate measurements of the airborne PM mass. In that work, the comparison of the amount of debris collected onto filters relative to the mass lost from the rotor and brake linings revealed that, under brake dynamometer operation, 70–90% of the wear debris became airborne. While this fraction remained nearly the same for the three lining types, the mass of airborne debris exhibited an approximately 4-fold variation. The present work extends the previous study in three ways: It provides (i) data on the particle size distributions, (ii) an analysis of the wear debris composition, and (iii) a comparison of brake dynamometer versus on-vehicle brake particle measurements. The data presented here update our knowledge about brake wear emissions, as the three brake lining formulations examined collectively represent about 90% of currently used automotive brakes.

Experimental Method

Brake Dynamometer Tests. Laboratory measurements of airborne brake wear particles were conducted using a programmable Link Compact Dynamometer (model 19), as previously described by Sanders et al. (4) Three lining type/vehicle combinations were tested that are representative of a wide range of current light-duty vehicles: low metallic/mid-size car, semimetallic/full-size truck, and non-asbestos organic/full-size car. The corresponding vehicle parameters used for the dynamometer are listed in Table 1. New brakes were obtained for each lining type and were run for > 1000 stops to “break them in” and achieve stable wear debris emissions.

Wear debris from these linings was measured using two sets of braking conditions. One is a set of 24 stops that are typical of urban driving, which we term the urban driving program (UDP). Test vehicles outfitted with accelerometers and brake rotor thermocouples provided the means to characterize these stops, as described in ref 4. The relevant velocities, deceleration rates, and initial brake temperatures (IBT) are recorded in Table 2 (the latter are recorded under roadway conditions and reflect the fact that the brakes do not cool to ambient temperature between stops). The stops in the UDP are relatively mild ($\leq 1.6\ \text{m/s}^2$) and occur at relatively slow speed ($< 90\ \text{km/h}$). Thus, a simulation of the Auto Motor and Sport magazine (AMS) vehicle braking test

* Corresponding author phone: (313)594-7527; fax: (313)322-7044; e-mail: mmaricq@ford.com.

TABLE 1. Dynamometer Vehicle Parameters

Lining →	low metallic	semimetallic	NAO
vehicle	mid-car	full-truck	full-car
rolling radius (mm)	303	369	319
effective radius (mm)	107	130	112
inertia (kg m ²)	45	90	50
wheel load (N)	4773	6454	4800
piston diameter (mm)	59	48	66
pistons	1	2	1

TABLE 2. Braking Parameters for Urban Dynamometer Program

stop	velocity (km/h)	deceleration (m/s ²)	car IBT (°C)	truck IBT (°C)
1	51	1.4	54	71
2	89	0.9	110	66
3	58	1.2	138	116
4	48	1.5	141	141
5	58	1.2	166	143
6	40	1.6	160	160
7	40	1.6	160	154
8	42	1.1	166	154
9	37	1.2	177	154
10	45	0.8	149	157
11	56	0.6	132	154
12	40	1.2	110	138
13	40	1.0	118	143
14	45	0.6	118	149
15	43	1.2	129	154
16	37	1.5	132	166
17	34	1.0	121	168
18	47	1.5	135	160
19	35	1.2	107	166
20	51	1.4	77	93
21	89	0.9	132	79
22	58	1.2	154	138
23	48	1.5	154	163
24	58	1.2	154	163

was performed to examine the nature of the wear debris under harsh braking conditions. The AMS test consists of 10 consecutive 7.9 m/s² stops from 100 to 0 km/h as quickly as the brake dynamometer can perform them. A limited number of tests consisting of a series of 1.8 m/s² stops from 96 km/h were also performed to provide a comparison between wear debris recorded using the brake dynamometer to the airborne debris measured behind a vehicle when the same stops are performed in a wind tunnel.

To allow quantitative determination of the airborne component of the brake wear, a hood was placed around the brake assembly, and a blower draws a constant flow of air past the brake assembly and into a 15.2 cm diameter duct (ref 4 provides a photograph of the apparatus). The average flow rate, as determined from the velocity distribution across the duct measured with a Pitot tube and inclined manometer, was typically set to ~3.6 m³/min (~3.3 m/s). After rising about 1 m, the air enters an approximately 2 m long horizontal tunnel. To allow the brake wear debris to be well mixed, samples are drawn onto filters and into the particle size instruments at distances greater than 10 tunnel diameters downstream from the 90° bend to the horizontal section.

Size Distribution and Mass Measurements. The total mass of airborne wear debris (reported here as mg stop⁻¹ brake⁻¹) was recorded by collection onto filter media (47-mm Emfab filters, Pall-Gelman), and particle size distributions were measured using a micro-orifice uniform deposit impactor (MOUDI, from MSP Corp.) and an electrical low-pressure impactor (ELPI, from Dekati Inc.). Isokinetic sampling for the filter and the ELPI, each of which operate at 10 L/min, is achieved by using 7.8 mm diameter probes. The probes enter the tunnel at an angle of 20° to minimize losses in tubing bends. The horizontal distance from the

sample point to the filter is 43 cm. The sample tube to the ELPI extends the same length and then bends an additional 70° to descend vertically ~50 cm to the ELPI inlet. A larger diameter tube of 1.27 cm provides nearly isokinetic sampling at the 30 L/min flow rate of the MOUDI. In this case, the horizontal portion of the sample line extends 25 cm before bending 70° to descend ~50 cm to the MOUDI inlet.

Both the ELPI and MOUDI are cascade impactors that separate particles according to their aerodynamic size. Grease-coated aluminum foils served as the collection substrates for both instruments, with the grease used to reduce particle bounce from one stage to the next. The MOUDI has 11 stages with D50% cut points of 56 nm, 100 nm, 180 nm, 320 nm, 560 nm, 1.0 μm, 1.8 μm, 3.2 μm, 5.6 μm, 10 μm, and 18 μm. In the case of the MOUDI, the foils were weighed before and after collection of the wear debris to determine directly the mass-weighted size distribution.

The ELPI was used to collect second by second size distributions. The ELPI operates by using a corona discharge to charge the particles prior to their introduction into the cascade impactor portion of the instrument (5). This portion can be operated in two modes. The mode utilized for this work included 13 stages with D50% cut points of 29 nm, 58 nm, 102 nm, 165 nm, 254 nm, 391 nm, 635 nm, 990 nm, 1.60 μm, 2.45 μm, 3.96 μm, 6.67 μm, and 10.12 μm. The second mode, which adds a filter stage to extend the lower size limit to ~5 nm at the expense of removing the 6.67-μm stage, was not chosen because of the lower resolution over the 1–10-μm range of interest to brake wear debris. As the particles within specific size ranges impact onto the corresponding stages, electrometers record the charge that is deposited. The resulting currents are converted to particle number concentrations by dividing by the charging efficiency, which depends on particle diameter, and correcting for particle losses on preceding stages (6). These, in turn, are converted to mass-weighted size distributions using an approximate value for the density of the brake wear debris (discussed below). The second by second data are integrated over the duration of the brake wear test and scaled by the number of stops to provide the number and mass distributions of particulate matter per stop. Finally, integration over the size distribution gives the total number and mass of wear particles generated per stop.

Brake Wear Debris Composition. As mentioned above, airborne wear debris from the UDP was collected on filter media. Heavier wear debris that settled on the hardware was brushed off and placed in a glass vial. In addition, wear debris collected on a piece of aluminum foil positioned below the rotor and caliper was also added to the glass vial. Using the same filter, vacuum supply, and flow control used for the airborne particle collection, some of the material collected in the glass vial was deposited on a filter for X-ray fluorescence analysis.

Both the airborne and hardware wear debris underwent elemental analysis. All samples (including a clean filter used for background subtraction) were cut to 38 mm diameter and mounted between 6 μm thick polypropylene films. The film supported the filter and kept the wear debris from moving within the spectrometer evacuation cycle. The analysis was carried out on a Phillips 2400 X-ray spectrometer equipped with a chromium tube and utilizing the UniQuant version 4 software. Characteristic peaks from the elements sodium to platinum were measured, and the background from the filter material was subtracted. After analysis of the spectra, the calculated mass of the wear debris was compared to the actual collected mass to ensure that the results were reasonable.

Ideally the filter samples are assumed to be thin films. At a typical filter loading of 10 mg, the average film thickness is ~2 μm, although individual particles range up to 20 μm.



FIGURE 1. Image of test vehicle showing location of sampling tubes. All positions shown, including a longer vertical tube reaching to the center of the wheel, were tested. The three positions were (i) along the wheel centerline extending to the cut-outs in the wheel covers (shown), (ii) at the axle (not shown), and (iii) in the wheel well behind the tire.

In practice, the heterogeneity of the particles could affect the fluorescence measurements due to outer layers of the particle absorbing radiation emitted from the interior (7). This depends on both the emitting and the absorbing elements. The thickness that yields a 10% absorption ranges from 5100 μm for Fe surrounded by C, to 42 μm for Cu surrounded by Fe, and to 0.05 μm for Si surrounded entirely by Fe. With the exception of Si surrounded by Fe, the film thickness for a 10% absorption is larger than $\sim 20 \mu\text{m}$; thus, with the possible exception of Si, the heterogeneity of the particles collected on the filter should have a minimal effect on the X-ray fluorescence measurements.

Wind Tunnel and Test Track Measurements. Two methods were used to compare the brake dynamometer data to wear debris measurements from a vehicle: tests conducted in a wind tunnel and measurements made driving on a test track. In the former case, a full-size car fitted with aggressive, low metallic brake linings underwent a series of 1.8 m/s^2 stops from 96 km/h and an IBT of 130 $^\circ\text{C}$ in a wind tunnel. For these tests, the wind speed was maintained at a constant 64 km/h, and the wind tunnel was operated in single pass airflow to avoid the accumulation of wear debris. The air enters the tunnel via a 4.7- m^2 rectangular nozzle and exits ~ 7 m behind the test vehicle. While the wind speed past the car under real-world stopping slows with vehicle speed, the use of a constant wind speed in the tunnel enables quantification of the brake wear debris that escapes the vehicle and becomes airborne.

A 0.4 cm diameter sample inlet was mounted at various heights and lateral positions at a distance of 5 m behind the vehicle and connected to the ELPI via a 1.9 cm diameter ~ 50 cm long Tygon tube. Particle size distributions were recorded at heights of 0.28, 0.56, and 0.98 m and at 0.0, 0.45, 0.90, and 1.20 m lateral displacement from the vehicle centerline in order to make a quantitative estimate of how much wear debris escapes the vehicle. The wind tunnel measurements are free from road dust since the vehicle remains stationary. The fact that particle emissions correlated with braking, but not acceleration, suggests that tire wear particles were not measurable, likely due to low wear from the smooth steel roller that supplies the load to the wheels.

An aerodynamic particle sizer (APS, from TSI, Inc.) was used to measure brake wear debris size distributions during braking events on the high speed track at the Dearborn Proving Grounds (DPC) and on public roads. This instrument was chosen because it could easily be run using the vehicle's 12 V electrical system. The engine vacuum supply for the vehicle ventilation system was tapped to provide airflow through the filter media. As shown in Figure 1, Tygon hoses running to 9 mm stainless steel tubes were connected to the exterior right side of the vehicle surrounding the front wheel. The vehicle was instrumented with a slip ring and rotor thermocouple to measure brake temperature on the left side so that the airflow was not disturbed on the right side. After screening all sampling positions for detectable dust levels, three positions were selected: inside the wheel, outside the wheel at the axle, and outside the wheel at the wheel cover openings. In addition, a tube was mounted directly onto the trailing edge of the caliper. All stops on the test track were made from 60 mph at decelerations of 0.15, 0.25, and 0.35 g. Each stop was repeated two times, and two different lining materials were tested (low metallic and NAO). The particulate matter collected by the APS was correlated with braking events and compared with the size distributions obtained from dynamometer testing.

Filters were installed in the vehicle with the low metallic linings while driving on public roads for 500 km. The debris was collected through the short vertical tube aligned with the wheel opening (Figure 1). After collection, the debris was analyzed by X-ray spectroscopy and compared to the analysis of the wear debris collected during the brake dynamometer tests. For the test track measurements, the particle sizer indicated a nonnegligible background during constant speed driving that can be attributed to road dust, and additional peaks roughly correlated to vehicle acceleration that might be associated with tire wear particles.

Results

Methods Comparison: ELPI, MOUDI, and Filter PM Mass. Conventional brakes reduce vehicle speed by using friction to convert kinetic energy into heat. In the process, abrasion

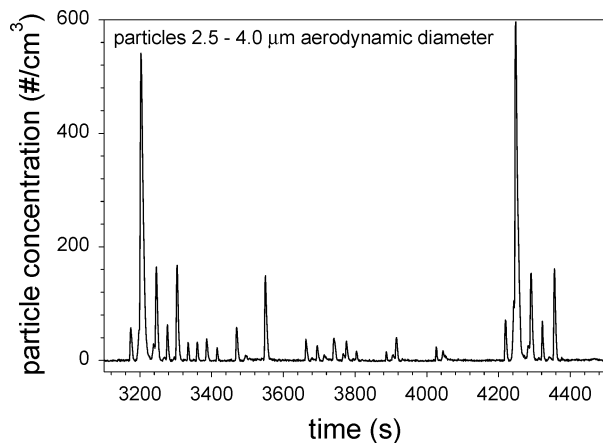


FIGURE 2. Brake wear debris concentration in the dilution tunnel recorded by the 2.5–4.0- μm ELPI impactor stage over one set of 24 stops of the UDP. The spacing between stops is determined by the time required for the rotor to reach the IBT for the succeeding stop.

of the brake linings and rotors produces wear debris in the micron size range, as illustrated in Figure 2 for the stops that comprise the UDP. There are a number of sampling issues that need to be addressed to ensure that reliable and unbiased measurements of the brake wear debris are made. For micron size particles, the primary loss mechanisms are by non-isokinetic sampling (impaction, for example, in bent sections of the sample line) and by gravitational settling. Because the measurements are made at ambient temperature, thermophoresis does not play a role, and diffusion is too slow in the micron size range to contribute to particle losses.

In the present measurements, the tunnel airflow rate and the sample probe diameters were chosen to closely match the tunnel and probe flow velocities at the 10 L/min flow rates of the filter sampler and ELPI and the 30 L/min flow rate of the MOUDI. This minimizes the loss of particles at the probe tip to $\leq 11\%$ for particles below 10 μm . Short tubes, with horizontal spans of 25–43 cm, were used to transport the sampled particles to the impactors to reduce gravitational losses. At a constant flow rate, large diameter tubes (low velocities) reduce losses in bends, whereas small diameter tubes (high velocities) reduce gravitational losses. Therefore the 1.27 diameter MOUDI probe diameter was increased to 2.54 cm prior to the 90° needed to introduce the particles into the impactor. Table 3 lists as a function of particle aerodynamic diameter the calculated transmission efficiencies for the filter, ELPI, and MOUDI. The details of these calculations are beyond the scope of the present paper. Interested readers are referred to Brockmann's (8) comprehensive discussion on the sampling and transport of aerosols for the expressions used to calculate the transport efficiencies. The filter sampling has an overall efficiency of $>80\%$ for particles $<10 \mu\text{m}$ diameter, which drops to $\sim 50\%$ by 20 μm . The MOUDI is similar, with an efficiency of $>86\%$ below 10 μm , which falls to 65% at 20 μm . The ELPI does not measure particles above 10 μm diameter. Its sampling efficiency increases from 67% at 10 μm to $>89\%$ below 5 μm .

Table 4 compares the PM mass of wear debris generated in brake dynamometer measurements of low metallic linings using both the 1.8 m/s² stops and the UDP. The MOUDI data are reported in two ways: (i) as the total mass and average diameter, which includes the masses recorded on all impactor stages, and (ii) as a PM₁₀ mass and average diameter, which

TABLE 3. Estimated Particle Losses Due to Gravitational Settling and Tubing Bends

measurement method	loss mechanism	flow rate (L/min)	sampling details	transport efficiency vs aerodynamic diameter ^{a,b}			
				20 μm	10 μm	5 μm	2 μm
filter	inlet	10	0.78 \times 10 cm	0.75 \pm 0.1	0.90 \pm 0.05	0.96 \pm 0.02	0.99 \pm 0.01
filter	gravity	10	0.78 \times 33 cm tube	0.83 \pm 0.03	0.95 \pm 0.02	0.99 \pm 0.01	0.99 \pm 0.01
filter	bend	10	20°, 0.78 cm d.	0.81 \pm 0.04	0.95 \pm 0.02	0.99 \pm 0.01	1.0
ELPI	inlet	10	0.78 \times 10 cm		0.90 \pm 0.05	0.96 \pm 0.02	0.99 \pm 0.01
ELPI	gravity	10	0.78 \times 33 cm tube		0.95 \pm 0.02	0.99 \pm 0.01	0.99 \pm 0.01
ELPI	bend	10	90°, 0.78 cm d.		0.78 \pm 0.02	0.94 \pm 0.01	0.99 \pm 0.01
MOUDI	inlet	30	1.27 \times 10 cm	0.74 \pm 0.1	0.89 \pm 0.05	0.96 \pm 0.02	0.99 \pm 0.01
MOUDI	gravity	30	1.27 \times 15 cm tube	0.95 \pm 0.02	0.99 \pm 0.01	1	1
MOUDI	bend	30	90°, 2.5 cm dia.	0.92 \pm 0.02	0.98 \pm 0.01	0.99 \pm 0.01	1.0

^a Efficiencies are calculated according to Brockmann (8). ^b Error bounds are estimated from the sensitivity of the efficiency to 10% variations of parameters including the tunnel to sample flow velocity ratio for the inlet efficiency, the sample flow rate for gravitational settling, and the sample flow rate and bend angle for transport through the bend.

TABLE 4. ELPI—MOUDI—Filter Comparison of Airborne Brake Wear Debris Mass^a

test	filter		MOUDI			ELPI	
	total mass (mg stop ⁻¹ brake ⁻¹)	total mass (mg stop ⁻¹ brake ⁻¹)	total mass mean d. (μm)	PM ₁₀ mass (mg stop ⁻¹ brake ⁻¹)	PM ₁₀ mass mean d. (μm)	PM ₁₀ mass (mg stop ⁻¹ brake ⁻¹)	PM ₁₀ mass mean d. (μm)
UDP	14	8.8	7.6	6.9	4.5	6.0	5.3
UDP	15	17	7.7	13	3.9	6.9	4.9
UDP	9.3	9.2	6.2	7.8	4.0	8.3	5.5
UDP	12	8.7	7.2	7.1	4.3	6.5	5.2
UDP		6.9	6.4	6.0	4.4	6.5	5.3
UDP	12					7.9	5.9
average	12	10	7.0	8.2	4.2	7.0	5.4
1.8 m/s ² decel	45	41	5.5	37	4.4	33	4.7
1.8 m/s ² decel	52	44	5.4	41	4.4	50	5.4
1.8 m/s ² decel	50	47	5.8	43	4.6	52	5.6
average	49	44	5.6	40	4.5	45	5.2

^a Brake dynamometer tests using low metallic brake linings.

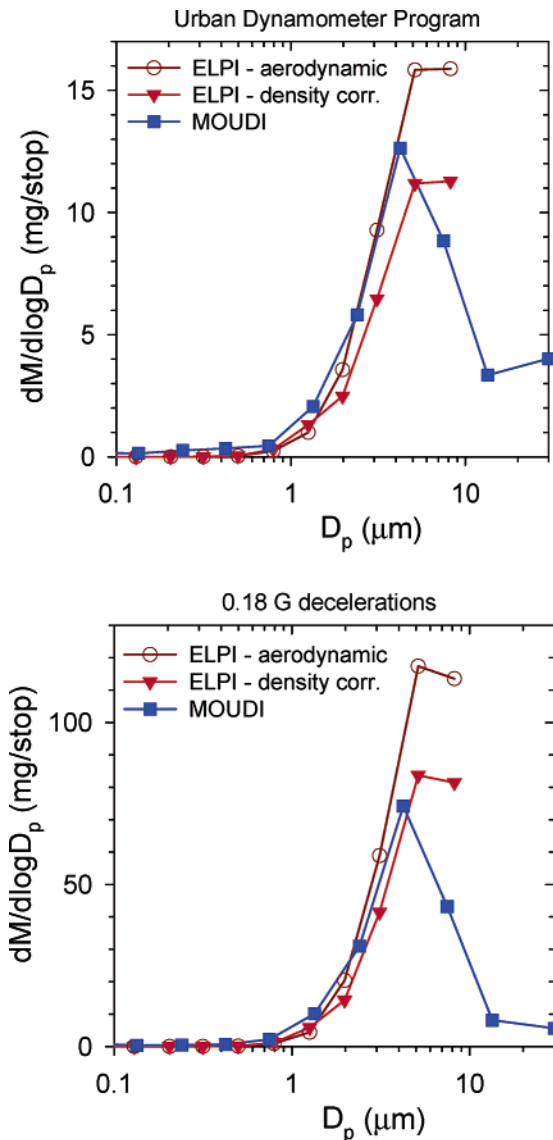


FIGURE 3. Comparison of the mass-weighted wear debris size distributions measured by the MOUDI and ELPI cascade impactors. Both the aerodynamic-based and density-corrected mass distributions calculated from the ELPI measurements are displayed.

include only the masses from impactor stages corresponding to diameters below $10\ \mu\text{m}$. The total mass can be compared to the filter samples, whereas the PM_{10} data are appropriate for comparison to the ELPI. The filter and MOUDI masses in Table 4 exhibit good agreement for both the UDP and the $1.8\ \text{m/s}^2$ stops. There are small differences that appear to be systematic, with the filter measurements leading to an average 15% higher PM mass most likely due to particle losses within the MOUDI.

To the lowest order, scaling the ELPI particle number distributions by $\pi/6D_p^3$ and a density of $1\ \text{g/cm}^3$ provides approximate mass distributions that in Figure 3 (open circles) compare favorably to the corresponding MOUDI mass distributions (squares) from the UDP tests and the $1.8\ \text{m/s}^2$ stops. However, the ELPI calculated masses underestimate the MOUDI data below $\sim 2\ \mu\text{m}$ and overestimate it at diameters larger than $2\ \mu\text{m}$. A more accurate conversion of the ELPI currents to a mass distribution is possible if one knows the density of the particles. Separate measurements of the material lost from the rotors and linings show that when low metallic linings are used, 60% of the wear debris comes from the rotor and 40% comes from the linings. Since

the rotor density is $7\ \text{g/cm}^3$ and the bulk density of the low metallic linings is $2.5\ \text{g/cm}^3$, we estimate that the wear debris has an average density of $5\ \text{g/cm}^3$. This allows the wear debris particle aerodynamic diameters, defined as equivalent unit density spheres, to be converted to Stokes diameters, equivalent spheres with the density of the bulk substance, via

$$D_{\text{st}} = D_{\text{aero}} \left(\frac{\rho_0 C_c(D_{\text{aero}})}{\rho_e C_c(D_{\text{mob}})} \right)^{1/2} \quad (1)$$

where $C_c = 1 + \lambda/D_p [2.34 + 1.05 \exp(-0.39 D_p/\lambda)]$ is the Cunningham slip correction (9), ρ_e is the effective particle density, $\rho_0 = 1\ \text{g/cm}^3$ represents unit density, and λ is the mean free path ($6.65 \times 10^{-6}\ \text{cm}$ for air at 1 atm).

Use of the Stokes diameter improves the determination of the mass distribution in two ways: (i) it is more appropriate than the aerodynamic diameter for calculation of the particle charging efficiency, and (ii) it provides a more direct conversion of the particle number distribution to a mass distribution. As illustrated in Figure 3 (and Table 4), the ELPI mass distributions calculated in this manner (solid triangles) improve the agreement with the MOUDI data (squares). Although small differences remain between the three PM measurement methods, it is reassuring that they provide a consistent characterization of the brake wear debris.

Lining Comparison: Low Metallic, Semimetallic, and Non-Asbestos Organic. The three lining types tested in this study differ considerably in the amount of airborne wear debris that is generated but exhibit similar distributions of particle sizes. As illustrated in Figure 4, the number-weighted distributions of the wear debris generated in the UDP test have broad maxima in the range of $0.5\text{--}2\ \mu\text{m}$, with tails that extend to $>10\ \mu\text{m}$. These distributions are calculated from the ELPI current distributions assuming average wear debris densities of 5, 4, and $3\ \text{g/cm}^3$, respectively, to determine the particle charging efficiency for the low metallic, semimetallic, and NAO linings. Three examples are provided for each lining type to demonstrate the test to test variability in the measured distributions. Typically a new set of linings produces a relatively high the amount of debris per stop, which decreases with successive stops by up to a factor of 2 and then levels off after about 1000 stops. The data presented in this paper are recorded after this initial “break-in” period. The major difference between the linings is that the low metallic linings generate 2–3 times the number of wear particles than the semimetallic and NAO linings. In the low metallic case, the particles are also larger by an average of about $0.5\ \mu\text{m}$.

As demonstrated in Figure 5, the large particle tails of the number distributions dominate the mass distributions. These exhibit a greater similarity between the lining types than do the number distributions. The peak in the mass distributions occurs at $\sim 6\ \mu\text{m}$ for all three linings. The approximately log-normal shape allows the distributions to be extrapolated beyond the $10\text{-}\mu\text{m}$ upper limit of the ELPI, as shown by the dotted lines in Figure 5. Table 5 compares filter and ELPI measurements of the average wear debris mass per stop generated from the three lining types in the UDP tests. The table lists both the PM_{10} mass calculated directly from the ELPI measurements and the total PM mass and mass-weighted mean diameter that are estimated from the extrapolated data. The total mass emissions extrapolated from the ELPI data are in good agreement with the filter measurements, within 25% on average. The mean particle size and the shape of the mass distribution are very similar for each of the three linings. But, the mass of wear debris from the UDP tests falls 4-fold from $\sim 8\ \text{mg stop}^{-1}\ \text{brake}^{-1}$ for the low metallic linings to $\sim 2\ \text{mg stop}^{-1}\ \text{brake}^{-1}$ for the semimetallic and NAO linings.

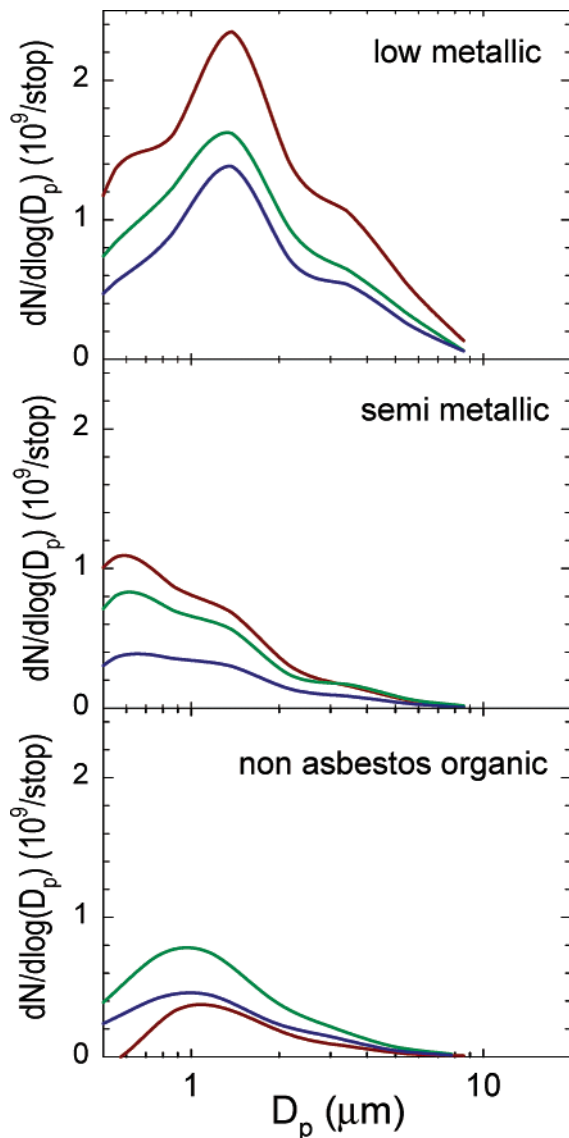


FIGURE 4. ELPI measurements of the number-weighted wear debris size distributions generated during the UDP from the low metallic, semimetallic, and NAO brake linings.

Wear debris generation during the AMS test differs considerably from the UDP test in the mass and size distribution of the particles and in the increasing amount of debris that is generated from one stop to the next. Figure 6 illustrates this trend in time and reveals an ~ 100 -fold increase in the number concentration of particles generated over the 10 sequential stops. Figure 7 shows that, in addition to the micron size wear particles characteristic of abrasion, the AMS test also generates a large number of submicron particles. In this case, the number-weighted size distribution is actually dominated by particles less than $0.3 \mu\text{m}$ in diameter. This size range is characteristic of aerosols generated chemically or by nucleation and condensation processes. In the case of brakes, these particles likely arise from the heat release and possible combustion of the organic materials used as binders in the brake linings, as brake temperatures rise to $500\text{--}600^\circ\text{C}$ during the AMS test, whereas they remain below $\sim 200^\circ\text{C}$ over the UDP test. Because of their small size, however, these submicron particles contribute little to the mass emissions, which are dominated by the mechanically generated wear particles (Figure 7B).

A comparison between the mass distributions in Figures 5 and 7 reveals a roughly 2 orders of magnitude increase in

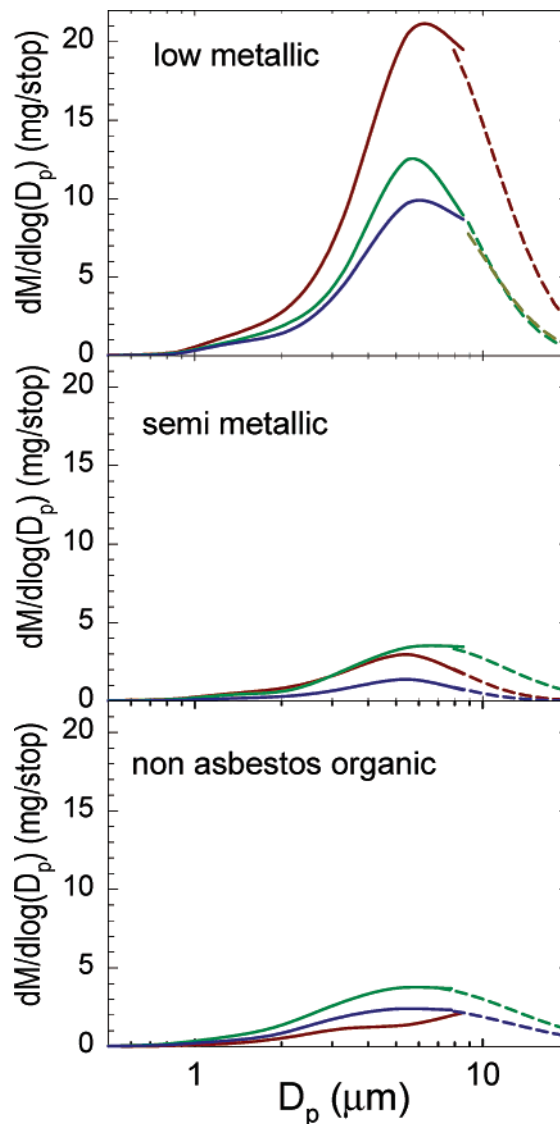


FIGURE 5. Density-corrected mass-weighted wear debris size distributions generated during the UDP from the low metallic, semimetallic, and NAO brake linings. Solid lines represent ELPI data. Dashed lines are log-normal extrapolations.

the mass of wear debris generated from the AMS test relative to the UDP test. The wear particles also appear to be on average larger for the AMS test, with a mass-weighted mean diameter near $10 \mu\text{m}$. The wear increase, however, is not uniform over the AMS test; instead, the debris mass increases from approximately $3 \text{ mg stop}^{-1} \text{ brake}^{-1}$ for the first few stops to over 3 g/stop for the final two stops. Presumably the increase in brake temperature that occurs because of quick succession of high deceleration stops explains the higher wear rates. Unlike for the UDP test, where the airborne PM constitutes 70–90% of the material lost from the rotor and linings, the filter collected wear debris represents only 20–50% of the loss in the AMS test (the fraction is deduced by recording the mass losses in the rotor and linings after a long series of stops, see ref 4). It is possible that a significant fraction of the wear debris surpasses $\sim 20 \mu\text{m}$ diameter and is inefficiently sampled from the dilution tunnel. It is possible that uncollected combustion products may also affect the mass balance.

Wear Debris Composition. The results from X-ray fluorescence analysis of the wear debris particles are shown in Figure 8. The elements with the highest concentration are Fe, Cu, Si, Ba, K, and Ti. In the semimetallic friction material,

TABLE 5. Comparison of Airborne Brake Wear Debris from Low Metallic, Semimetallic and Non-Asbestos Organic Linings (Brake Dynamometer Tests)

test	filter	ELPI		
	total mass (mg stop ⁻¹ brake ⁻¹)	estd total mass ^a (mg stop ⁻¹ brake ⁻¹)	mass mean d. ^a (μm)	PM10 mass (mg stop ⁻¹ brake ⁻¹)
Low Metallic				
UDP	11.7	13	6.2	10.7
UDP	6.9	7	5.5	6.1
UDP	8.0	7	5.5	6.1
UDP	6.2	6	6.0	5.1
average	8.2	8.3	5.8	7.0
Semimetallic				
UDP	2.1	1.7	5.2	1.6
UDP	2.0	2.1	6.2	1.7
UDP	2.0	2.5	6.2	2.0
UDP	2.0	1.6	5.2	1.5
average	2.0	2.0	5.7	1.7
Non-Asbestos				
UDP	1.1		~5	0.9
UDP	2.6	3.1	5.7	2.4
UDP	1.8	1.7	5.3	1.3
average	1.8	2.4	5.5	1.5

^a Obtained from the mass-weighted ELPI size distribution extrapolated to include particles above 10 μm in diameter.

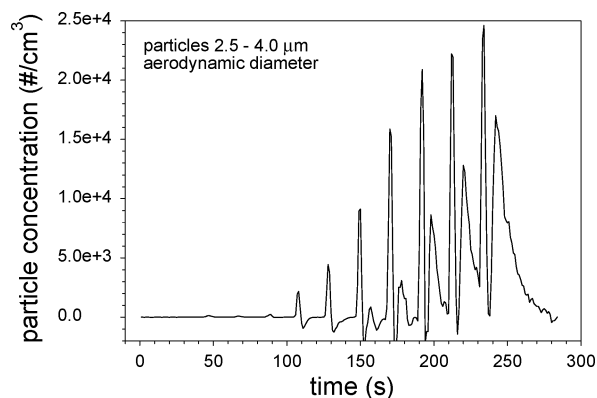


FIGURE 6. Brake wear debris concentration in the dilution tunnel recorded by the 2.5–4.0-μm ELPI impactor stage over the 10-stop AMS test.

the iron is primarily from the iron powder and steel wool in the lining. For both semimetallic and NAO linings, most of the wear is from the linings (90% and 70%, respectively). For the low metallic system, which contains abrasives, the Fe is primarily from cast iron rotor wear, which contributes 60% of the total PM mass. Copper is a high-temperature lubricant present to some degree in almost all linings. Silicon is present in the rotor, and silica is sometimes present in the lining as an abrasive. Barium sulfate is a common friction modifier. Potassium titanate fibers are present as a strengthener in the NAO lining.

The composition of the airborne debris and the debris that sticks to the hardware is very similar in most cases. This implies that there is negligible segregation of any elemental ingredient during the wear process. For example, we do not observe a significantly different concentration of any element in the finer airborne debris than in the coarser hardware debris. The NAO brake measurements reveal a few elements (Si, Ba) for which airborne versus hardware composition differences are observed. Although these differences may be real, the NAO also produces the lowest quantity of wear debris; thus, the analysis may not be as accurate as for the

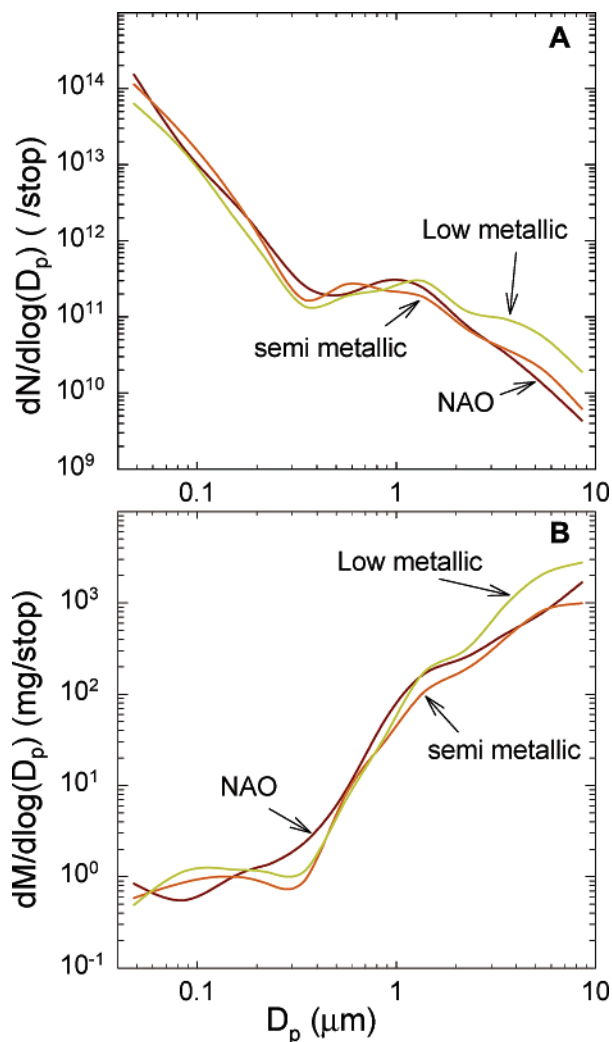


FIGURE 7. Number-weighted (A) and density-corrected mass-weighted (B) wear debris size distributions averaged over the first three AMS stops.

other two lining types. The present elemental analysis is consistent with the presence of high Fe, Cu, and Ba concentrations being a fingerprint of brake dust in the environment, such as used by Sternbeck et al. (10) in their roadway tunnel study of metal emissions.

Organic material was not specifically measured, but its contribution can be examined indirectly. For the UDP stops a separate submicron particle mode is not observed; thus, one could assume that the organic fraction of the PM mass is approximately equal to the organic fraction in the brake linings, weighted for the lining contribution to the overall lining + rotor PM mass. In the AMS test, an extreme non-real-world test, a separate submicron PM mode is observed that is similar to a combustion aerosol and, therefore, is likely to be dominated by organic material. However, its contribution to the PM mass remains negligible (Figure 7B).

Vehicle Measurements: Wind Tunnel and Test Track. The airflow around the brake hardware mounted on a dynamometer is not representative of the flow past the brakes on a vehicle. This raises the question of how much of the brake wear debris, which is of the size that can become airborne, escapes from the vehicle. Because of the complicated pattern, the airflow under a vehicle is very difficult to reproduce other than by actually driving the vehicle on a roadway. Unfortunately, in this case quantitative measurement of the PM wear debris becomes problematic. Here, we follow two approaches: In the first case we record the brake

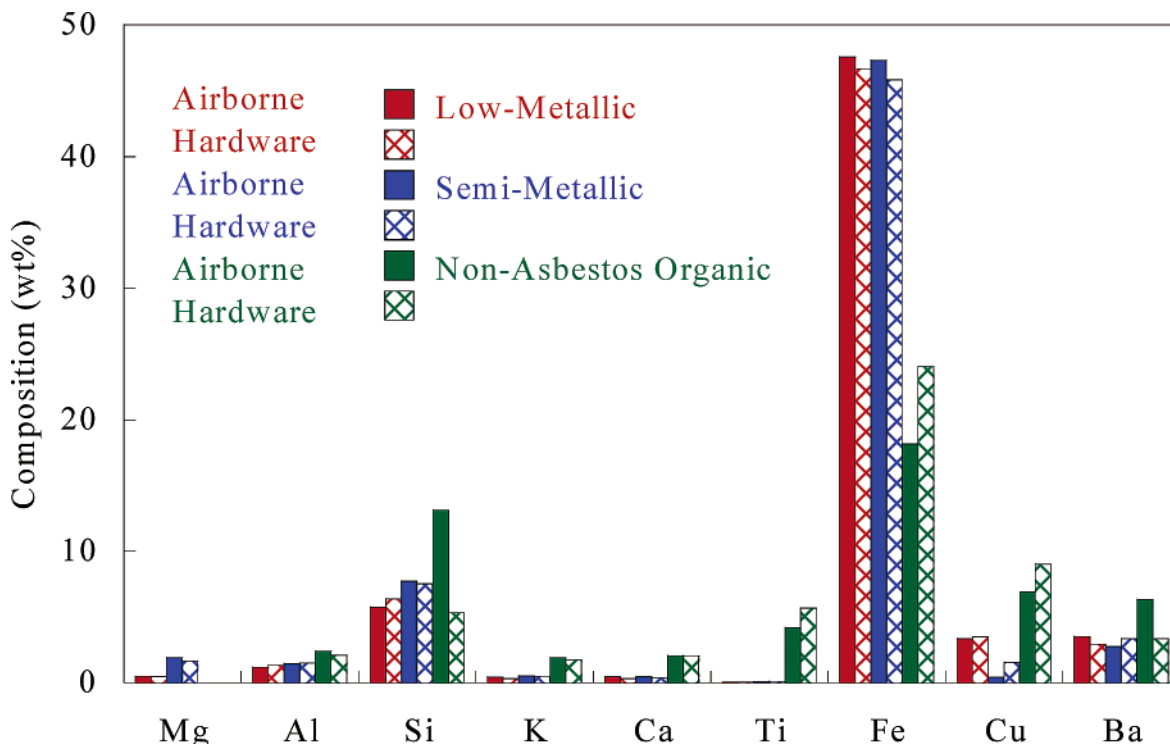


FIGURE 8. Elemental analysis of the airborne wear debris from low metallic, semimetallic, and non-asbestos organic brakes. Both the lining and rotor contributions are presented.

wear behind a vehicle operated in a wind tunnel, and in the second case we make onboard measurements of brake particles generated by stops performed on a test track.

The wind tunnel tests fall short of “real world” measurements in two ways: Unlike when driving, the floor is stationary with respect to the vehicle, and in the present tests we maintain a constant wind speed of 64 km/h even though the 1.8 m/s² stops are applied at 96 km/h. However, the wind tunnel is considerably more realistic than the brake dynamometer tests, and by maintaining a constant wind speed, we are able to map the flux of brake wear particles behind the vehicle as they pass a plane perpendicular to the wind direction. Integration of this flux over the duration of the stop and over the cross section of the wind tunnel then provides a means to quantify the amount of debris that escapes the vehicle.

Figure 9A depicts the momentary increases in particulate matter above the ambient wind tunnel background level that occur upon application of the brakes. Typically the PM from 5 stops was recorded and averaged at each position behind the vehicle. The measurements were made 5 m behind the vehicle at 3 heights above the tunnel floor and at 4 lateral positions from the vehicle centerline to 30 cm beyond the side of the vehicle, with the assumption of symmetry about the centerline. Weighting the ELPI size distributions by particle mass and integrating over particle diameter provides an estimate of the mass of debris (PM₁₀) at each location, as illustrated in Figure 9B. As might be expected, the highest particle concentrations are located behind the wheels. Similar results were obtained at 1.6 m behind the vehicle (not shown) and at 5 m (Figure 9). Integration over the wind tunnel cross section yields ~21 mg stop⁻¹ brake⁻¹ of wear debris (with the aggressive low metallic linings). Comparison to Table 4 leads to the conclusion that for the full-size test car used here approximately 50% of the brake wear escapes the vehicle. This is consistent with brake dynamometer tests in which a wheel is mounted in addition to the brake hardware and which shows that 50–70% of the airborne brake wear escapes the wheel (4).

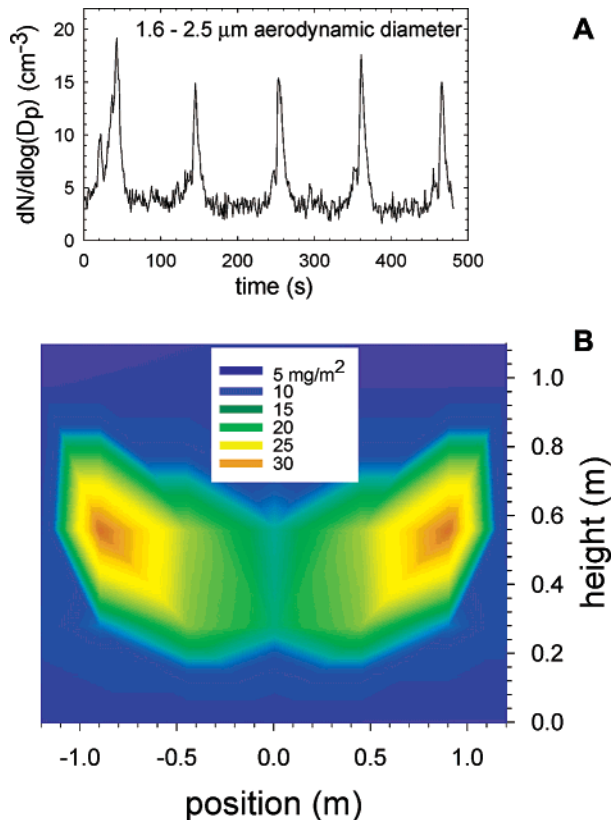


FIGURE 9. Brake wear debris measured in the wind tunnel. Panel A shows the 1.6–2.5- μm debris recorded over a succession of 1.8 m/s² stops from 96 km/h. Panel B displays the mass flux of brake wear debris through a cross section of the wind tunnel located 5 m behind the test vehicle.

The primary goals of the real-world test track measurements were to detect brake particle emissions during vehicle operation, to correlate particulate emissions with braking

TABLE 6. Comparison of Wear Debris Composition from Road versus Dynamometer Testing of Low Metallic Linings

	road (wt %)	dyno (wt %)		road (wt %)	dyno (wt %)
Mg	0.8	0.5	Ti	0.1	0.1
Al	1.7	1.2	Fe	22.2	47.6
Si	15.3	5.8	Cu	1.2	3.4
K	2.8	0.4	Ba	8.0	3.5
Ca	3.9	0.5			

events, and to show that the size distributions and composition of the wear debris is similar to that found in dynamometer testing. In fact, micron size particle emissions were observed and directly correlated with braking events. The particle size distributions for the three lining types are similar to the laboratory brake dynamometer measurements in Figure 5; however, the mass-weighted mean diameter decreases from approximately 6 μm for the laboratory measurements to about 3 μm in the test track data. This is expected from the non-isokinetic sampling and transport losses (including bends needed to route the tubing, see Figure 1) that were necessary to collect brake wear debris during vehicle operation, noting that these losses increase with particle size.

The composition of the wear debris collected during the test track experiments is compared in Table 6 to the dynamometer data. The ratio of Fe to Cu is similar in the two samples; however, Si, K, Ca, and Ba are significantly higher in the roadway sample. One complication from roadway tests is interference from re-entrained road dust. This may explain the higher levels of Si, K, and Ca, but the reason for the relatively high roadway Ba value is unclear.

Discussion

There are only a few previous studies of airborne brake wear with which to compare the present results, and many of these pertain to asbestos linings (2, 11, 12). Garg et al. (3) measured particle size distributions and mass emissions of wear debris using modern semimetallic and NAO linings, but their results differ in a number of respects from the present work. For example, they obtain a smaller fraction of airborne wear than we do, and their wear particle size distributions vary considerably from one lining type to another, whereas the present results do not.

To interpret the present measurements as well as future work, it is important to explore the possible origins of these discrepancies. A likely explanation originates from the difficulties inherent in sampling and transporting micron size particles in an unbiased manner. The present work emphasizes the use of isokinetic sampling and a shallow entry angle of the probe into the dilution tunnel to minimize sampling losses, which are particle size dependent. Relatively large diameter tubing is used to reduce losses in the 90° bend required to transport the wear particles to the ELPI and MOUDI. The measurements of Garg et al. (3) sampled brake wear particles using a flow rate of 18.4 L/min through a 0.64 cm diameter probe inserted at 90°. This leads to two mechanisms of particle loss: non-isokinetic sampling (the tunnel vs probe flow velocity ratio is 0.1–0.4) and impaction in the 90° bend. Under these sampling conditions, each mechanism leads to an approximately 25% particle loss calculated at 5 μm . Thus, the predicted net particle loss is ~45% at 5 μm , which increases for larger particles and decreases for smaller particles. Garg et al. (3) reported that, with the wheel assembly mounted on the dynamometer, ~35% of the wear debris became airborne. If this value is corrected for the estimated sampling losses, it increases the airborne fraction to ~64%, a value that becomes consistent

with the 50–70% airborne fraction we obtain for dynamometer measurements that include a wheel (4).

The mass mean diameter of the brake wear debris reported by Garg et al. (3) varies from 0.7 to 2.5 μm . In contrast, the present UDP test data yields a mass mean diameter of about 6 μm , as based on either the MOUDI or extrapolated ELPI data. The AMS tests produce large numbers of submicron particles that originate from the release and burning of organic materials; yet the mass remains dominated by the wear particles and the mass mean diameter increases to near 10 μm . Two factors likely contribute to these conflicting results: First, in the micron size range particle losses tend to increase with particle size. Thus, measurements with sampling losses yield apparent mean diameters smaller than the actual value. The present sampling system was designed to avoid such losses and, therefore, yields larger mean particle sizes. (However, our test track measurements, described above, were affected by such losses.) Second, we employ greased substrates in the present study. This reduces particle bounce and shifts the distribution to the more correct, larger size.

In addition to the sampling and transport efficiency calculations (Table 3 and above), there are two consistency checks that support the present wear debris size and mass measurements. When the mass of wear debris that is recovered from the brake hardware and the surface below the brake is added to the mass of the 70–90% airborne fraction (dynamometer measurements), the sum agrees well with the mass loss measured from the rotor and lining weights. Second, the wear debris masses calculated from the MOUDI and ELPI size distributions are consistent with the filter collection, which supports the mass-weighted mean diameter of 6 μm .

MOBILE6 expresses brake PM emissions as $\text{BRAKE} = 0.0128 \times \text{PSBRK}$, where BRAKE is the g/mi emission rate and PSBRK is the fraction of PM mass with diameter smaller than a specified cutoff (*l*). The fractions and cutoffs are 0.98 at 10 μm , 0.90 at 7 μm , 0.82 at 4.7 μm , 0.16 at 1.1 μm , and 0.09 at 0.43 μm . This emissions factor is applied to all light-duty vehicles and brake formulations without consideration of composition. The results of this study differ from the MOBILE6 brake debris description in three ways: (i) the emission levels from distinct brake formulations vary by up to a factor of 4, (ii) the PM composition varies with brake type, and (iii) the assumed cumulative size distribution differs from the experimental data.

In contrast to the MOBILE6 cumulative size distribution, the present results yield fractions and cutoffs of 0.8 at 10 μm , 0.6 at 7 μm , 0.35 at 4.7 μm , 0.02 at 1.1 μm , and <0.01 at 0.43 μm for the UDP stops typical of urban driving. The main differences are a 20% fraction of particles >10 μm and a smaller fraction of submicron particles than assumed by the model. In an average sense, the 13 mg/mi PM₁₀ emission factor is consistent with the present measurements. However, brake formulations are designed to fulfill a number of design parameters aimed at their primary function, namely, stopping the vehicle. As a secondary consequence, both the emission level and the composition can vary. For example, relative to NAO linings, low metallic linings exhibit higher levels of wear debris and a larger fraction of that is iron.

Both the wind tunnel and test track experiments reveal that brake wear debris escapes the vehicle and enters the atmosphere. Once airborne, micron size particles are removed from the atmosphere by gravitational settling and deposition. The controlled conditions of the wind tunnel allow the airborne fraction entering to be quantified at approximately 50% of the rotor plus lining mass loss for the test vehicle used in this work. This fraction is consistent with the 50–70% result obtained when we add a wheel to the brake dynamometer and to the ~64% derived from the

corrected data of Garg et al. (3) This percentage is not surprising considering the losses by impaction that one might expect in the airflow between the brakes and the vehicle exterior. However, these fractions are rough estimates. Actual values will depend on vehicle design, wheel and wheel cover design (open versus closed), and vehicle operating conditions.

Acknowledgments

The authors thank Andy Drews, Mark Jagner, and David Benson for their insights and help with the X-ray analysis of the filter collected brake wear debris.

Literature Cited

- (1) United States Environmental Protection Agency. EPA420-R-03-001; 2003. <http://www.epa.gov/otaq/m6.htm>.
- (2) Cha, S.; Carter, P.; Bradow, R. L. *SAE Tech. Pap.* **1983**, No. 831036.
- (3) Garg, B.; Cadle, S. H.; Groblicki, P. J.; Mulawa, P. A.; Laroo, C.; Parr, G. A. *Environ. Sci. Technol.* **2000**, *32*, 4463.
- (4) Sanders, P. G.; Dalka, T. M.; Xu, N.; Maricq, M. M.; Basch, R. H. *SAE Tech. Pap.* **2002**, No. 2002-01-1280.

- (5) Keskinen, J.; Pietarinen, K.; Lehtimäki, M. *J. Aerosol Sci.* **1992**, *23*, 353.
- (6) Marjamäki, M.; Keskinen, J.; Chen, D.-R.; Pui, D. Y. H. *J. Aerosol Sci.* **2000**, *31*, 249.
- (7) Lachance, G. R.; Claisse, F. *Quantitative X-ray Fluorescence Analysis*; John Wiley & Sons: New York, 1995.
- (8) Brockmann, J. E. In *Aerosol Measurement*; Willeke, K., Baron, P. A., Eds.; Van Nostrand Reinhold: New York, 1993; pp 77–111.
- (9) Hinds, W. C. *Aerosol Technology*; John Wiley & Sons: New York, 1999; p 49.
- (10) Sternbeck, J.; Sjödin, Å.; Andréasson, K. *Atmos. Environ.* **2002**, *36*, 4735.
- (11) Jacko, M. G.; DuCharme, R. T.; Somers, J. H. *SAE Tech. Pap.* **1973**, No. 730548.
- (12) Williams, R. L.; Muhlbaier, J. L. *Environ. Res.* **1982**, *29*, 70.

Received for review February 18, 2003. Revised manuscript received June 5, 2003. Accepted June 16, 2003.

ES034145S